STRUCTURAL BIOLOGY COMMUNICATIONS

ISSN 2053-230X

Crystal structure of the human mitochondrial amidoxime-reducing component 1 M187K variant

Charlotte M. Rehbein, Michel A. Struwe* and Axel J. Scheidig*

Structural Biology, Zoological Institute, Kiel University, Am Botanischen Garten 1–9, 24118 Kiel, Germany. *Correspondence e-mail: mstruwe@strubio.uni-kiel.de, axel.scheidig@strubio.uni-kiel.de

Received 26 May 2026
Accepted 4 November 2026

Edited by M. J. Romao, Universidade Nova de Lisboa, Portugal

Keywords: molybdenum cofactor; mARC; lipid metabolism; MASLD; MASH.

PDB reference: human mARC1 M187K variant, 29aj

Supporting information: this article has supporting information at journals.iucr.org/f

The human mitochondrial amidoxime-reducing component 1 (mARC1) is a molybdenum-dependent enzyme whose protein-coding variants confer protection against common metabolic liver diseases. Whereas the frequent A165T variant acts largely through accelerated cellular degradation, the basis of protection by the rarer M187K variant remains obscure, as it has been reported that there are no differences between the wild-type and M187K-variant protein in terms of cellular protein levels and localization. Here, the crystal structure of the human mARC1 M187K variant, crystallized as a T4 lysozyme fusion after iterative micro-seeding, was determined at 1.63 Å resolution. The variant structure is essentially superimposable with the previously reported wild-type and A165T structures, with pairwise root-mean-square deviations of 0.3–0.4 Å, and the pentacoordinated molybdenum cofactor is fully intact. Differential scanning fluorimetry across a broad pH range revealed only a modest, pH-dependent decrease in thermal stability associated with the exchange, most pronounced at alkaline pH. These data suggest that the disease-protective effect of M187K is unlikely to originate from gross structural rearrangement or active-site perturbation.

1. Introduction

The human mitochondrial amidoxime-reducing component enzymes mARC1 and mARC2 (gene names *MTARC*1 and *MTARC*2) are molybdoenzymes that were originally discovered due to their role in activating *N*-hydroxylated prodrugs of amidines, for example novel oral anticoagulants (Clement & Struwe, 2023; Havemeyer *et al.*, 2006), and are recognized as a biotransformation pathway for pharmaceutical drugs (Klopp *et al.*, 2024). Later, a potential involvement in lipid metabolism was suggested (Neve *et al.*, 2012, 2015) and further supported by the phenotype observed in a murine knockout model, where mice with an *Mtarc2*$^{-/-}$ genotype showed strong alterations in lipid metabolism compared with wild-type animals and a remarkable resistance towards high-fat diet-induced obesity (Rixen *et al.*, 2019).

Interest in mARC enzymes has increased dramatically in recent years, after it was discovered that coding variants of mARC1 confer protection against common liver diseases such as metabolic dysfunction-associated steatotic liver disease (MASLD) and metabolic dysfunction-associated steatohepatitis (MASH) (Emdin *et al.*, 2020), including decreased liver-related mortality (Schneider *et al.*, 2021). How mARC enzymes are linked to lipid metabolism and even what their physiological substrates are, and the extent to which mARC1 and mARC2 are isofunctional, remains unknown (Struwe *et al.*, 2023).

The most common variant detected among study populations is A165T and consequently this variant has received the

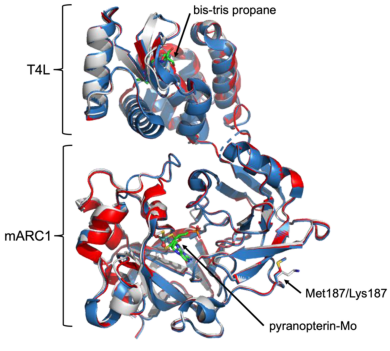

OPEN ACCESS
Published under a CC BY 4.0 licence

most attention. mARC1 protein with the A165T amino-acid exchange has essentially the same structure as the wild-type protein (Struwe *et al.*, 2022). However, in a biological context, mARC1 A165T is still considered a loss-of-function variant for practical purposes, as it shows increased cellular degradation of the protein and thus strongly depleted mARC1 protein levels (Dutta *et al.*, 2024; Hou *et al.*, 2024).

Genome-wide association studies have detected another single amino-acid exchange variant, M187K, which is much rarer than A165T, but appears to confer protection against liver diseases in a very similar fashion (Emdin *et al.*, 2020). Interestingly, cell-culture models show that while *MTARC*1 mRNA levels were similar for cells expressing wild-type, A165T- and M187K-variant mARC1, only A165T led to lower mARC1 protein levels and potentially mis-localization of the protein. On the other hand, the M187K-variant protein is detected at similar levels as the wild-type protein and is seen correctly co-localized with mitochondria (Wu *et al.*, 2024; Smagris *et al.*, 2024; Coyne *et al.*, 2025).

Early *in vitro* characterization of heterologously expressed mARC variants did not identify A165T or M187K as protein variants with markedly impaired molybdenum-cofactor loading or *N*-reductive activity against the model substrate benzamidoxime (Ott *et al.*, 2014). For the A165T protein variant, it is now well established that accelerated protein degradation leads to lower effective protein levels *in cellulo*, and this is thought to be central to the lipid phenotype. The picture is much less clear for the rarer M187K variant that displays a similar phenotype but no changes in degradation or localization.

Here, we determined the crystal structure of the mARC1 M187K protein variant at near-atomic resolution. While obtaining diffraction-quality crystals was somewhat more challenging than for the wild-type and A165T variants, the structure itself is virtually indistinguishable from previously reported mARC1 structures.

2. Materials and methods

Standard methods were used for all molecular-biology procedures (Ausubel *et al.*, 2003). Unless stated otherwise, all chemicals were purchased from Carl Roth GmbH+Co. KG (Karlsruhe, Germany) and were of >99% purity or of the highest purity available.

2.1. Macromolecule production

The pQE80-based expression plasmid for the hmARC1-T4L fusion protein carrying the p.M187K variant was generated by site-directed mutagenesis of the previously described plasmid (Kubitza, Ginsel *et al.*, 2018). This crystallization construct encodes an N-terminally truncated, soluble variant of human mARC1 comprising residues 53–337 (285 amino acids), in which the hydrophobic membrane anchor was removed. To facilitate crystallization, a full-length T4 lysozyme (T4L; residues 1–161) was internally inserted into hmARC1, replacing the native residues Ala129 and Tyr130 between positions 128 and 131, resulting in an overall fusion-protein length of 455 amino acids (including spacers and the C-terminal 6×His-tag). Mutagenesis was achieved using the Q5 site-directed mutagenesis kit (New England Biolabs #E0554) according to the manufacturer's instructions with the mutagenic primers 5′-CGAGCCTCACAAACGACCGAG AC-3′ and 5′-AAGTGCACCAGGCGG-3′, which had been designed using the *NEBaseChanger* web tool (https://nebasechanger.neb.com). Successful mutagenesis was confirmed by Sanger sequencing using the primers 5′-GTATCACGAGGC CCTTTCGTCT-3′ and 5′-CATTACTGGATCTATCAACAG GAG-3′.

Heterologous expression was performed in the molybdopterin-accumulating *Escherichia coli* strain TP1001 (Palmer *et al.*, 1996). Briefly, bacteria were grown at 37°C in Terrific broth supplemented with 1 m*M* Na_2MoO_4, 0.1 m*M* ferric citrate, 0.5 m*M* $MgSO_4$, 0.5 m*M* $MgCl_2$, 5 m*M* NH_4Cl and 100 µg ml^{-1} carbenicillin until an apparent OD_{600} of ∼0.2 was measured. The incubation temperature was reduced to 22°C and 0.05 m*M* isopropyl β-D-1-thiogalactopyranoside was added to induce expression. After 22 h, the cells were harvested by centrifugation, flash-frozen in liquid nitrogen and stored at −80°C until further use.

The cells were resuspended in purification buffer [50 m*M* NaH_2PO_4, 300 m*M* NaCl, 10 m*M* Na_2MoO_4, 10%(*w*/*v*) glycerol pH 7.4] supplemented with 0.7 m*M* phenylmethylsulfonyl fluoride (PMSF) and a catalytic amount of deoxyribonuclease I (VWR #A3778). The cells were lysed by two passages through an Emulsiflex C3 high-pressure homogenizer (Avestin) and cell debris was removed by centrifugation. The lysate was loaded onto a HiTrap TALON Crude 1 ml column (Cytiva #29048565) equilibrated in purification buffer and connected to an ÄKTApure 25M low-pressure chromatography system (Cytiva). Nonspecifically bound proteins were washed from the column with 10 ml 15 m*M* imidazole in purification buffer, followed by elution of the target protein with a linear gradient from 15 to 375 m*M* imidazole over 20 ml. Fractions were analysed by SDS–PAGE, pooled, concentrated using a spin concentrator (Carl Roth #25TL) and exchanged into storage buffer [50 m*M* Tris–HCl, 150 m*M* NaCl, 5%(*w*/*v*) glycerol pH 6.8] using a PD-10 desalting column (Cytiva #17085101). Macromolecule-production information is summarized in Table 1.

2.2. Crystallization

In contrast to the T4 lysozyme-fusion proteins of wild-type mARC1 and its A165T variant, which crystallized spontaneously within two days, the M187K variant protein did not crystallize spontaneously. Diffraction-quality crystals were obtained through one round of cross-seeding with the wild-type construct and two rounds of microseeding with the M187K variant. All crystals were obtained by hanging-drop vapour diffusion on glass cover slips (Carl Roth #P235.1) over 24-well crystallization plates (Molecular Dimensions #MD3-11) sealed with silicone grease (Carl Roth #0856.1). The wild-type protein was crystallized against a reservoir consisting of

Table 1
Macromolecule-production information.

Source organism	*Homo sapiens* (hmARC1), *Enterobacteria* phage T4 (T4 lysozyme)
Expression vector	Modified pQE-80 (Qiagen)
Expression host	*Escherichia coli* TP1001 (Palmer *et al.*, 1996)
Complete amino-acid sequence†	MQQVGTVAQLWIYPVKSCKGVPVSEAEC TAMGLRSGNLRDRFWLVINQEGNMVTA RQEPRLVLISLTCDGDTLTLSAMNIFE MLRIDEGLRLKIYKDTEGYYTIGIGHL LTKSPSLNAAKSELDKAIGRNCNGVIT KDEAEKLFNQDVDAAVRGILRNAKLKP VYDSLDAVRRCALINMVFQMGETGVAG FTNSLRMLQQKRWDEAAVNLAKSRWYN QTPNRAKRVITTFRTGTWDAYTKDLLL PIKTPTTNAVHKCRVHGLEIEGRDCGE AAAQWITSFLKSQPYRLVHFEPH**K**RPR RPHQIADLFRPKDQIAYSDTSPFLILS EASLADLNSRLEKKVKATNFRPNIVIS GCDVYAEDSWDELLIGDVELKRVMACS RCILTTVDPDTGVMSRKEPLETLKSYR QCDPSERKLYGKSPLFGQYFVLENPGT IKVGDPVYLLGQGTVDHHHHHH

† Underlined, T4 lysozyme; bold, exchanged residue.

100 m*M* bis-tris propane–HCl pH 6.5, 20 m*M* sodium molybdate, 27.5%(*w*/*v*) PEG 3350. Once well ordered crystals had grown, the crystal suspension was crushed using a rounded-tip glass rod and transferred into a 1.5 ml reaction tube containing 100 µl freshly prepared reservoir to create a seed stock, and a serial dilution in 1:10 steps ranging from 1:10 to 1:1 000 000 was prepared. These seed stocks were used to initiate crystallization of M187K-variant mARC1-T4L in hanging drops consisting of 2 µl hmARC1 protein solution (concentration 6 mg ml^{-1}), 1 µl reservoir and 1 µl seed solution. Crystals obtained from the 1:10 000 dilution droplet were once again used to prepare seed stocks, using an optimized reservoir composition of 100 m*M* bis-tris propane–HCl pH 8.0, 20 m*M* Na_2MoO_4, 27.5% PEG 3350, 10 m*M* tris(2-carboxyethyl) phosphine hydrochloride (TCEP), and crystals were obtained from droplets prepared from 2.5 µl protein solution, 1 µl reservoir solution and 0.5 µl seed solution. Finally, crystals from the 1:10 000 dilution of this second round were used for a third round of seeding (using the same dilution range). Crystals originating from the 1:100 000 dilution droplet of this final round were suitable for X-ray diffraction experiments two days after setup. Crystallization information is summarized in Table 2.

Table 2
Crystallization.

Method	Hanging-drop vapour diffusion
Plate type	24-well plate (Molecular Dimensions #MD3-11)
Temperature (K)	291
Protein concentration (mg ml^{-1})	6
Buffer composition of protein solution	50 m*M* Tris–HCl pH 6.8, 150 m*M* NaCl, 5%(*w*/*v*) glycerol
Composition of reservoir solution	100 m*M* bis-tris propane–HCl pH 8.0, 20 m*M* Na_2MoO_4, 27.5% PEG 3350, 10 m*M* tris(2-carboxyethyl)phosphine hydrochloride (TCEP)
Volume and ratio of drop	4 µl (2.5 µl protein, 1 µl reservoir, 0.5 µl seed stock)
Volume of reservoir (µl)	1000

Table 3
Data collection and processing.

Values in parentheses are for the outer shell.

Diffraction source	P13, PETRA III, DESY
Wavelength (Å)	0.9762
Temperature (K)	100
Detector	EIGER X 16M, Dectris
Crystal-to-detector distance (mm)	229.328
Rotation range per image (°)	0.1
Total rotation range (°)	360
Exposure time per image (s)	0.01
Space group	$P2_12_12_1$
a, *b*, *c* (Å)	60.99, 75.07, 110.66
α, *β*, *γ* (°)	90, 90, 90
Mosaicity (°)	0.121
Resolution range (Å)	62.12–1.63
No. of unique reflections	64043
Completeness (%)	99.9 (99.7)
Multiplicity	13.6
$\langle I/\sigma(I)\rangle$	8.5 (2.2)
R_{merge}	0.190 (1.148)
$CC_{1/2}$	0.989 (0.790)
Overall *B* factor from Wilson plot (Å^2)	25.56

2.3. Data collection and processing

An intergrown crystal (see Fig. 1*c*) was broken and one fragment was transferred into a 5 µl droplet of fresh reservoir solution. After approximately 45 s, the crystal was mounted into a CryoLoop (Hampton Research) without addition of further cryoprotectant and flash-cooled in liquid nitrogen. X-ray diffraction data were collected on the P13 beamline operated by EMBL at DESY, Hamburg (Cianci *et al.*, 2017), equipped with an EIGER 16M detector (Dectris). Diffraction data were indexed and integrated with *XDS* (Kabsch, 2010), followed by scaling and merging with *AIMLESS* (Evans & Murshudov, 2013). The high-resolution limit was set to 1.63 Å, where the outer-shell $\langle I/\sigma(I)\rangle$ is 2.2 and $CC_{1/2}$ is 0.790. Data-collection and processing statistics are summarized in Table 3.

2.4. Structure solution and refinement

Phasing was achieved by molecular replacement with *Phaser* (McCoy *et al.*, 2007) using the structure of wild-type mARC1-T4L (PDB entry pdb_00006fw2). The structure was refined using *Phenix AutoBuild* (Terwilliger *et al.*, 2008), *phenix.refine* (Afonine *et al.*, 2012) and interactive model building in *Coot* (Emsley *et al.*, 2010). The model and structure factors have been deposited in the RCSB Protein Data Bank under accession code pdb_000029aj. Refinement statistics are summarized in Table 4.

2.5. Differential scanning fluorimetry

In order to assess the impact of the M187K protein variant on the overall stability of mARC1, we compared wild-type and M187K-variant proteins by differential scanning fluorimetry (DSF). For these assays, mARC1 constructs without the internal T4 lysozyme fusion were used. Site-directed mutagenesis was achieved using the same primers as for the crys-

Table 4
Structure solution and refinement.

Resolution range (Å)	62.12–1.63 (1.66–1.63)
Completeness (%)	99.9 (99.7)
No. of reflections, working set	60912 (2714)
No. of reflections, test set	3131 (136)
Final R_{cryst}	0.188 (0.239)
Final R_{free}	0.215 (0.283)
No. of non-H atoms	
Total	4214
Protein	3563
Ligand	67
Water	584
R.m.s. deviations	
Bond lengths (Å)	0.010
Angles (°)	1.054
Average *B* factors (Å^2)	
Protein	30.5
Ligand	35.5
Solvent	37.1
Ramachandran plot	
Most favoured (%)	97.5
Allowed (%)	2.5
Outliers (%)	0.00

tallization construct and the protein was purified by immobilized metal-affinity chromatography as described above. For DSF analysis, the protein was diluted to a concentration of approximately 1 mg ml^{-1} in storage buffer. 4 µl of 5000× SYPRO Orange (Thermo Fisher #S6650) were added to 1.1 ml protein solution (final concentration ∼18×). 10 µl of this solution were distributed into a 96-well RT-PCR plate (Sarstedt #72.1979.102) and mixed with 10 µl buffer concentrates from the Durham pH Screen (Molecular Dimensions #MD1-101), before sealing the plate with a transparent film (Sarstedt 95.1999). Melting curves were recorded through the TAMRA channel of an ABI7300 RT-PCR instrument (Thermo Fisher). Briefly, fluorescence intensity was measured between 21 and 75°C, with 0.25 min equilibration time at each temperature followed by 1 min readout time. Melting temperatures were determined as the inflection point of a Boltzmann sigmoidal curve fitted to the data using *Excel for Mac* 16.107 (Microsoft) and *Prism for macOS* 11.0.0 (GraphPad), following a standard procedure described elsewhere (Huynh & Partch, 2015). Assays were performed as technical duplicates to assess the reproducibility of the results.

3. Results and discussion

3.1. Diffraction-quality crystals of M187K-variant mARC1 protein are obtained after multiple rounds of micro-seeding

In contrast to wild-type (Kubitza, Ginsel *et al.*, 2018) and A165T (Struwe *et al.*, 2022) mARC1-T4L fusion proteins, our preparation of the M187K variant of the same construct did not initially generate any crystals in hanging-droplet vapour-diffusion experiments using solutions that had worked for the other two variants. However, the M187K variant did form crystals when a seed stock was prepared from crystals of the wild-type construct. Initially, these cross-seeded crystals were very thin needles with visible growth defects (Fig. 1*a*). Size and morphology improved markedly when these crystals were used for another round of seeding (Fig. 1*b*) and diffraction-quality crystals were eventually obtained from a third round of seeding (Fig. 1*c*).

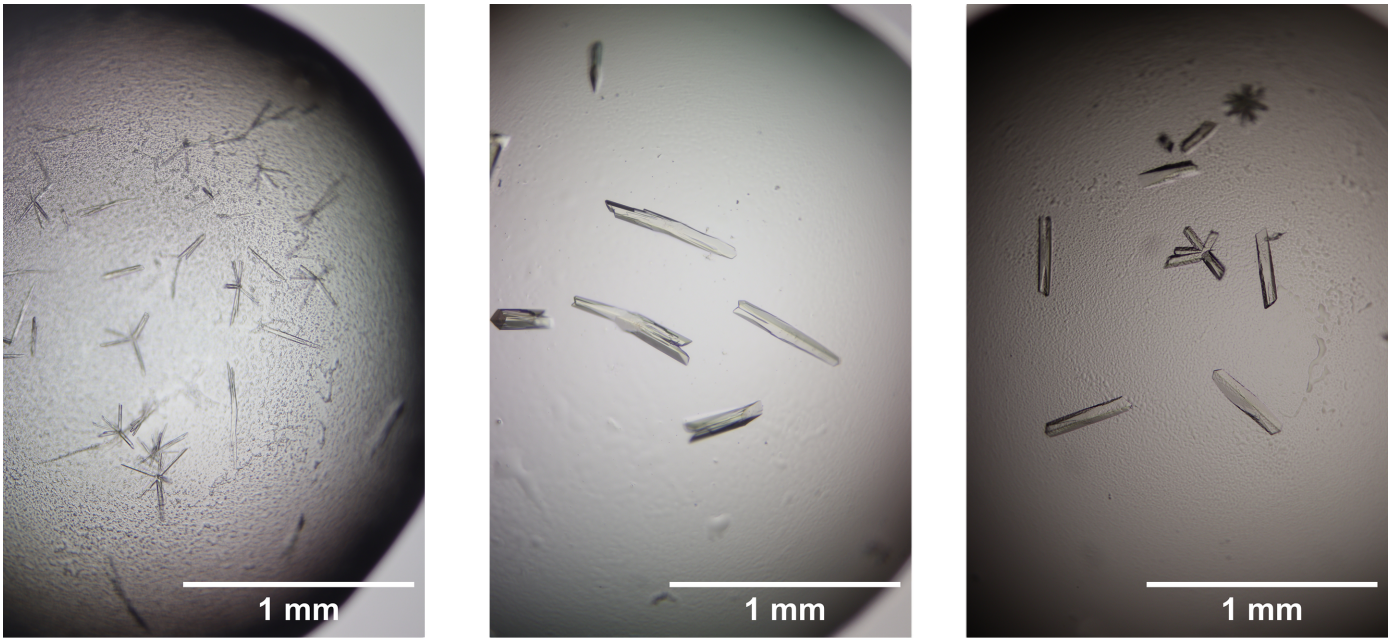

(*a*) (*b*) (*c*)

Figure 1
Crystals formed by M187K-variant mARC1-T4L. (*a*) After micro-seeding with crushed crystals of wild-type mARC1-T4L, (*b*) after micro-seeding with crushed crystals from the droplet shown in (*a*) and (*c*) after micro-seeding with crushed crystals from the droplet shown in (*b*). Crystal morphology gradually improves over multiple rounds of seeding. The crystal used for structure determination was a fragment of the intergrown crystal seen at the centre of (*c*).

3.2. Wild-type, M187K- and A165T-variant proteins share the same three-dimensional structure

The structure of the M187K variant of mARC1 was solved by molecular replacement and refined, with the refinement statistics shown in Table 4.

We subsequently performed structural comparisons of the three mARC1 variants using the *DALI* web server (Holm *et al.*, 2023). The r.m.s.d. values for the pairwise comparison of the M187K variant (this study) with wild-type mARC1 (PDB entry pdb_00006fw2) and A165T-variant mARC1 (PDB entry pdb_00007p41) are reported at 0.4 and 0.3 Å resolution, respectively. Visual inspection of the overlaid models shows that, apart from the side chain of Met187/Lys187, the three structures are virtually identical to each other (Fig. 2*a*). In order to verify that the crystallized species is the M187K variant, both lysine and methionine were modelled and refined for residue 187. When methionine (wild-type) rather than lysine (variant of interest) is fitted, a strong negative peak appears in the difference map, confirming that we are indeed looking at crystals of the M187K-variant protein (Figs. 2*b* and 2*c*). Electron density for the prosthetic group shows an intact pentacoordinated $[MoO_2(S_{Cys})(PDT)]^-$ cofactor, which is consistent with structures derived from spectroscopic data on human mARC1 and its *E. coli* homologue YcbX (Struwe *et al.*, 2024; Yang *et al.*, 2023) and previously published X-ray crystal structures of mARC1 variants (Struwe *et al.*, 2022; Kubitza, Bittner *et al.*, 2018). Overall, the active site of mARC1 seems unaffected by the M187K amino-acid exchange (Fig. 2*d*). Given that the distance between the catalytic molybdenum ion and the C^{α} atom of Met187/Lys187 is some 26 Å (similar to the distance between the molybdenum ion and Ala165/Thr165), it is not necessarily expected that the amino-acid substitution would affect the active site. Nonetheless, it is worth documenting that no such perturbation is observed.

3.3. The M187K amino-acid exchange has a modest pH-dependent effect on thermal stability

The Durham pH screening kit comprises 93 different buffer conditions (28 individual buffer substances, spanning a pH range from 4 to 11). mARC1 displays optimal stability at acidic or near-neutral pH, with melting temperatures decreasing noticeably at alkaline pH. This general stability profile is observed both for the wild-type and M187K-variant proteins. However, we do notice that the M187K variant

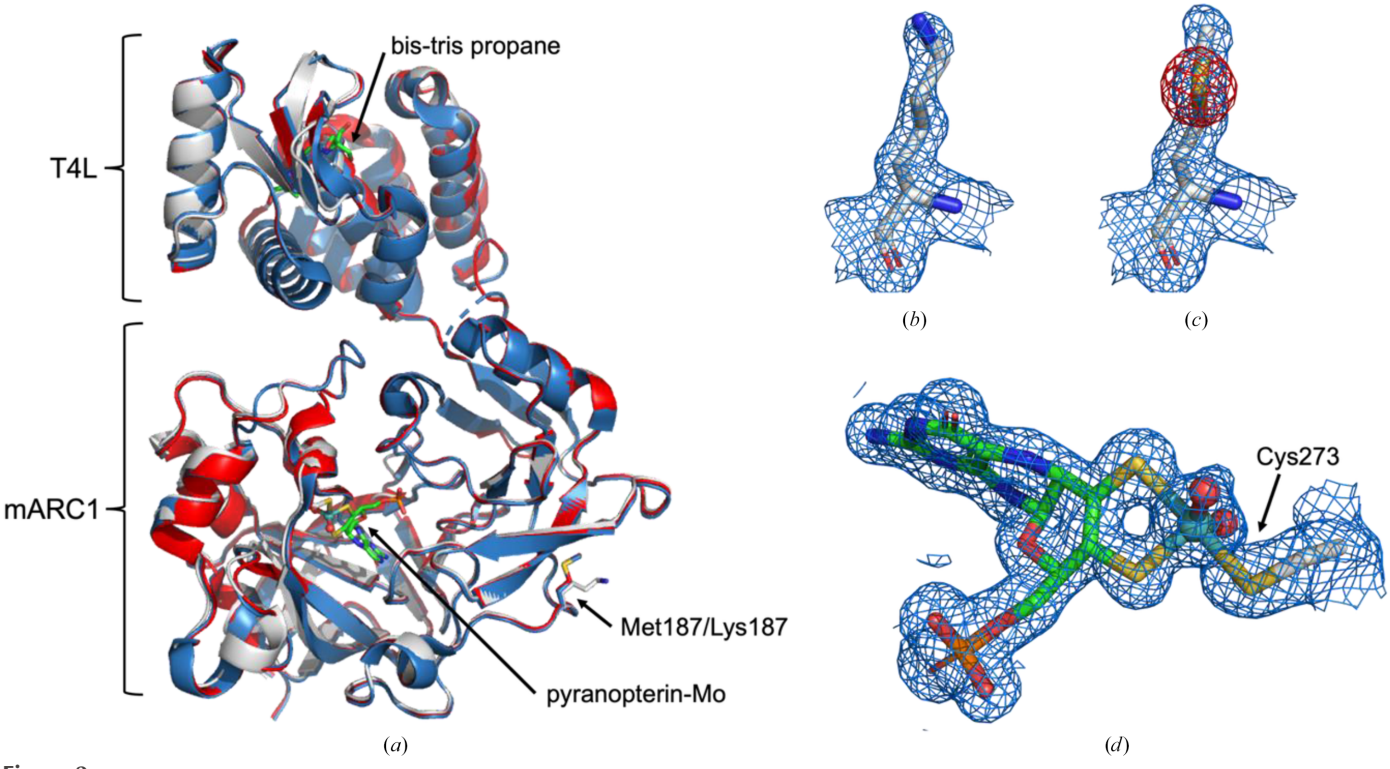

Figure 2
(*a*) Overlay of the structure reported here (all shown in ribbon representation: grey, M187K variant), PDB entry pdb_00006fw2 (blue, mARC1 wild type) and PDB entry pdb_00007p41 (red, mARC1 A165T variant). The structures are virtually indistinguishable from one another, with the only relevant differences being observed at the actual mutation sites. The stick representation within the T4 lysozyme (T4L) region shows a bound bis-tris propane molecule from the crystallization buffer. The dashed line represents the two hmARC1 residues substituted by T4 lysozyme. (*b*, *c*) Electron-density maps for the side chain of residue 187, when (*b*) the residue is a lysine during refinement or (*c*) the residue is refined as a methionine (according to the wild-type species). $2mF_o - DF_c$ maps are displayed as a blue mesh at a contour level of 1σ. $mF_o - DF_c$ maps are displayed as red (negative density) and green (positive density) meshes at a contour level of 4σ. If this residue is refined as a methionine, a strong negative peak at the methionine thioether sulfur (S^{δ}) is observed. (*d*) $2mF_o - DF_c$ omit electron-density map in which the pyranopterin–molybdenum cofactor has been fitted and displayed in stick representation, and the molybdenum as well as its terminal oxygen ligands in sphere representation (C atoms in green, O atoms in red, N atoms in blue, S atoms in yellow, P atoms in orange and Mo atoms in light blue) shows the prosthetic group fully intact. Molecular visualizations and figures were generated using *PyMOL* (version 3.1.0, Schrödinger).

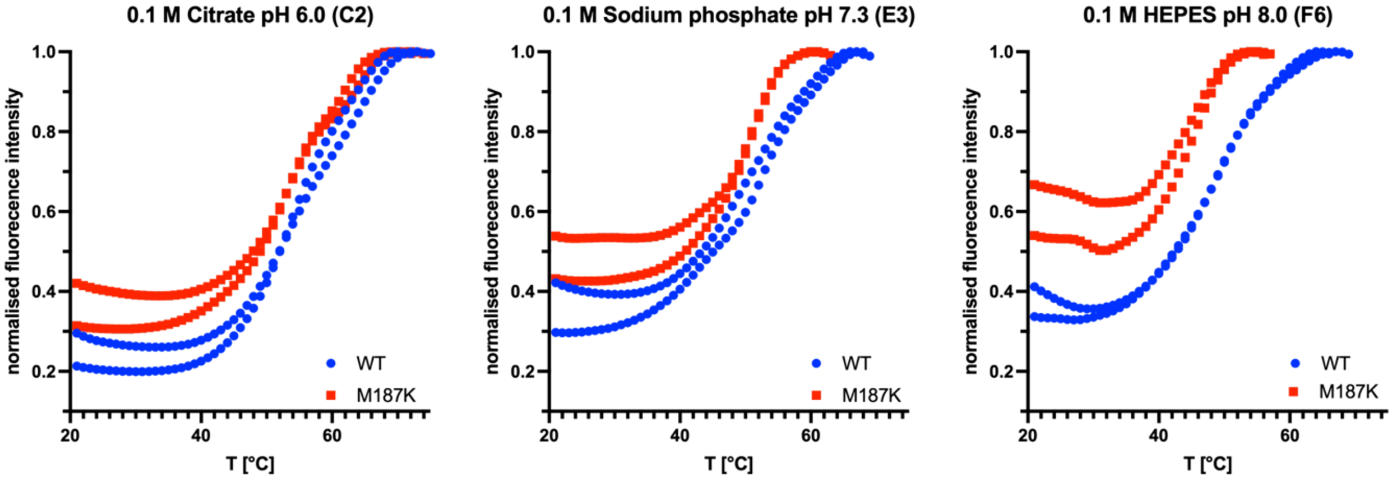

Figure 3
Example melting curves of wild-type (WT) and M187K-variant mARC1 at three example pH values. Blue points represent melting curves recorded for the wild-type protein and red squares represent melting curves recorded for the M187K-variant protein. For clarity, curves were normalized to the peak intensity. Curves recorded for the M187K variant are shifted to lower temperatures and generally display higher initial fluorescence, consistent with the amino-acid exchange decreasing thermal stability. This effect becomes more pronounced as the pH increases.

appears generally less stable compared with the wild-type protein. The effect is small at acidic pH but becomes stronger as the pH increases. Example melting curves at different pH values are presented in Fig. 3. All estimated melting temperatures and their correlation with buffer pH are displayed in Supplementary Figs. S1 and S2.

While these data suggest a modest destabilizing effect of the M187K amino-acid exchange, it should be noted that at pH values likely to be biologically relevant (6–8) both wild-type and M187K-variant mARC1 can be considered to be quite stable proteins, with estimated melting temperatures of the protein generally higher than 45°C. When *N*-reductive activities of various mARC1 protein variants, including wild type and M187K, were investigated using *in vitro* enzyme activity assays, these were performed at optimized reaction conditions in 20 m*M* 2-(*N*-morpholino)ethanesulfonic acid (MES) pH 6.0 at 37°C, and no significant differences in enzymatic activity (determined as the generation of HPLC-quantified benzamidine from benzamidoxime) were observed (Ott *et al.*, 2014). This is consistent with observations made by DSF, *i.e.* both variants being very stable in acidic MES buffer (T_m > 50°C).

In summary, DSF data do not support the conclusion that decreased thermal stability of the M187K variant would be responsible for a loss of function under physiological circumstances that would clarify the variant's influence on hepatic lipid accumulation. The slight decrease in thermal stability may, however, explain why multiple rounds of microseeding were necessary in order to obtain crystals that diffracted to high resolution for the M187K variant, consistent with reports that DSF can be predictive for crystallization behaviour and diffraction quality (Sato & Senda, 2026).

4. Conclusion

In conclusion, the M187K substitution does not induce a detectable rearrangement of the mARC1 fold or molybdenum-cofactor site in the crystallographic construct used here. The variant does, however, display altered crystallization behaviour and a modest pH-dependent reduction in thermal stability. The presented data do not support the hypothesis that the disease-protective phenotype of the M187K amino-acid exchange is caused by large-scale structural disruptions or perturbations of the active site.

Acknowledgements

We gratefully acknowledge access to the core facilities of the BiMo/LMB of Kiel University and thank Brigitte Bittner for technical assistance. The synchrotron data were collected on the P13 beamline operated by EMBL Hamburg at the PETRA III storage ring (DESY, Hamburg, Germany). We would like to thank Michael Agthe for the assistance in using the beamline. GPT-5.5 was used for assistance with spelling, grammar and stylistic refinement. All scientific content, interpretation and conclusions are the responsibility of the authors. Open access funding enabled and organized by Projekt DEAL.

References

Afonine, P. V., Grosse-Kunstleve, R. W., Echols, N., Headd, J. J., Moriarty, N. W., Mustyakimov, M., Terwilliger, T. C., Urzhumtsev, A., Zwart, P. H. & Adams, P. D. (2012). *Acta Cryst.* D**68**, 352–367.
Ausubel, F. M., Brent, R., Kingston, R. E., Moore, D. D., Seidman, J. G., Smith, J. A. & Struhl, K. (2003). *Current Protocols in Molecular Biology*. New York: John Wiley & Sons.
Cianci, M., Bourenkov, G., Pompidor, G., Karpics, I., Kallio, J., Bento, I., Roessle, M., Cipriani, F., Fiedler, S. & Schneider, T. R. (2017). *J. Synchrotron Rad.* **24**, 323–332.
Clement, B. & Struwe, M. A. (2023). *Molecules*, **28**, 4713.
Coyne, E. S., Nie, Y., Lee, D., Pandovski, S., Yang, T., Zhou, H., Rosahl, T. W., Carballo-Jane, E., Abdurrachim, D., Zhou, Y., Hendra, C., Ali, A. A. B., Meyers, S., Blumenschein, W., Gongol, B., Liu, Y., Zhou, Y. & Talukdar, S. (2025). *Hepatol. Commun.* **9**, e0637.

Dutta, T., Sasidharan, K., Ciociola, E., Pennisi, G., Noto, F. R., Kovooru, L., Kroon, T., Lindblom, A., Du, Y., Pirmoradian, M., Wallin, S., Mancina, R. M., Lindén, D. & Romeo, S. (2024). *Liver Int.* **44**, 1219–1232.
Emdin, C. A., Haas, M. E., Khera, A. V., Aragam, K., Chaffin, M., Klarin, D., Hindy, G., Jiang, L., Wei, W. Q., Feng, Q., Karjalainen, J., Havulinna, A., Kiiskinen, T., Bick, A., Ardissino, D., Wilson, J. G., Schunkert, H., McPherson, R., Watkins, H., Elosua, R., Bown, M. J., Samani, N. J., Baber, U., Erdmann, J., Gupta, N., Danesh, J., Saleheen, D., Chang, K. M., Vujkovic, M., Voight, B., Damrauer, S., Lynch, J., Kaplan, D., Serper, M., Tsao, P., Million Veteran Program, Mercader, J., Hanis, C., Daly, M., Denny, J., Gabriel, S. & Kathiresan, S. (2020). *PLoS Genet.* **16**, e1008629.
Emsley, P., Lohkamp, B., Scott, W. G. & Cowtan, K. (2010). *Acta Cryst.* D**66**, 486–501.
Evans, P. R. & Murshudov, G. N. (2013). *Acta Cryst.* D**69**, 1204–1214.
Havemeyer, A., Bittner, F., Wollers, S., Mendel, R., Kunze, T. & Clement, B. (2006). *J. Biol. Chem.* **281**, 34796–34802.
Holm, L., Laiho, A., Törönen, P. & Salgado, M. (2023). *Protein Sci.* **32**, e4519.
Hou, W., Watson, C., Cecconie, T., Bolaki, M. N., Brady, J. J., Lu, Q., Gatto, G. J. Jr & Day, T. A. (2024). *J. Biol. Chem.* **300**, 107353.
Huynh, K. & Partch, C. L. (2015). *Curr. Protoc. Protein Sci.* **79**, 28.9.1–28.9.14.
Kabsch, W. (2010). *Acta Cryst.* D**66**, 125–132.
Klopp, C., Zhang, X., Campbell, M. K., Kvaskoff, D., Struwe, M. A., Warren, C. R., Bajrami, B., Scheidig, A. J., Jones, A. K. & Clement, B. (2024). *J. Med. Chem.* **67**, 18090–18097.
Kubitza, C., Bittner, F., Ginsel, C., Havemeyer, A., Clement, B. & Scheidig, A. J. (2018). *Proc. Natl Acad. Sci. USA*, **115**, 11958–11963.
Kubitza, C., Ginsel, C., Bittner, F., Havemeyer, A., Clement, B. & Scheidig, A. J. (2018). *Acta Cryst.* F**74**, 337–344.
McCoy, A. J., Grosse-Kunstleve, R. W., Adams, P. D., Winn, M. D., Storoni, L. C. & Read, R. J. (2007). *J. Appl. Cryst.* **40**, 658–674.
Neve, E. P., Köfeler, H., Hendriks, D. F., Nordling, A., Gogvadze, V., Mkrtchian, S., Näslund, E. & Ingelman-Sundberg, M. (2015). *PLoS One*, **10**, e0138487.
Neve, E. P., Nordling, A., Andersson, T. B., Hellman, U., Diczfalusy, U., Johansson, I. & Ingelman-Sundberg, M. (2012). *J. Biol. Chem.* **287**, 6307–6317.
Ott, G., Reichmann, D., Boerger, C., Cascorbi, I., Bittner, F., Mendel, R. R., Kunze, T., Clement, B. & Havemeyer, A. (2014). *Drug Metab. Dispos.* **42**, 718–725.
Palmer, T., Santini, C.-L., lobbi-Nivol, C., Eave, D. J., Boxer, D. H. & Giordano, G. (1996). *Mol. Biol.* **20**, 875–884.
Rixen, S., Havemeyer, A., Tyl-Bielicka, A., Pysniak, K., Gajewska, M., Kulecka, M., Ostrowski, J., Mikula, M. & Clement, B. (2019). *J. Biol. Chem.* **294**, 17593–17602.
Sato, Y. & Senda, T. (2026). *IUCrJ*, **13**, 169–183.
Schneider, C. V., Schneider, K. M., Conlon, D. M., Park, J., Vujkovic, M., Zandvakili, I., Ko, Y. A., Trautwein, C., Center, R., Carr, R. M., Strnad, P., Thaiss, C. A. & Rader, D. J. (2021). *Med*, **2**, 851–863.
Smagris, E., Shihanian, L. M., Mintah, I. J., Bigdelou, P., Livson, Y., Brown, H., Verweij, N., Hunt, C., Johnson, R. O., Greer, T. J., Hartford, S. A., Hindy, G., Sun, L., Nielsen, J. B., Halasz, G., Lotta, L. A., Murphy, A. J., Sleeman, M. W. & Gusarova, V. (2024). *PLoS Genet.* **20**, e1011179.
Struwe, M. A., Clement, B. & Scheidig, A. (2022). *Hepatol. Commun.* **6**, 3277–3278.
Struwe, M. A., Scheidig, A. J. & Clement, B. (2023). *J. Biol. Chem.* **299**, 105306.
Struwe, M. A., Yang, J., Kolanji, K., Mengell, J., Scheidig, A. J., Clement, B. & Kirk, M. L. (2024). *Inorg. Chem.* **63**, 19063–19073.
Terwilliger, T. C., Grosse-Kunstleve, R. W., Afonine, P. V., Moriarty, N. W., Zwart, P. H., Hung, L.-W., Read, R. J. & Adams, P. D. (2008). *Acta Cryst.* D**64**, 61–69.
Wu, M., Tie, M., Hu, L., Yang, Y., Chen, Y., Ferguson, D., Chen, Y. & He, A. (2024). *Biochem. Biophys. Res. Commun.* **702**, 149655.
Yang, J., Struwe, M., Scheidig, A., Mengell, J., Clement, B. & Kirk, M. L. (2023). *Inorg. Chem.* **62**, 5315–5319.